## **International Journal of Technology**

http://ijtech.eng.ui.ac.id



Research Article

# Synthesis, Characterization, and Conductivity Evaluation of CuNP-rGO-PANI Nanocomposites for Printed Sensors

Priska Wisudawaty 1,2, Endang Warsiki 1,\*, Sugiarto 1, Taufik Djatna 1

Abstract: Nanocomposites composed of copper nanoparticles (CuNP), reduced graphene oxide (rGO), and polyaniline (PANI) have garnered considerable attention owing to their actantial as conductive materials for printed sensor applications. This study aims to synthesize CuNP-rGO-PANI nanocomposites through a chemical reduction method and examine their structural, morphological, and electrical properties. The synthesis process involves reducing graphene oxide (GO) using sodium borohydride (NaBH<sub>4</sub>), followed by the incorporation of CuNP and PANI through in situ polymerization. The synthesized nanocomposites were characterized using Fourier-transform infrared (FTIR) spectroscopy, Raman spectroscopy, and scanning electron microscopy (SEM) to verify their chemical composition and morphological structure. Additionally, the electrical conductivity of the CuNP-rGO-PANI nanocomposites was evaluated to determine their feasibility for use in printed sensors. Raman spectroscopy results reveal that the incorporation of Cu nanoparticles increases the ID/IG ratio, indicating a rise in structural defects within rGO. SEM analysis determined that the average particle size of the CuNP-rGO-PANI nanocomposite is approximately 11.48 nm. FTIR characterization further demonstrates that the addition of CuNPs alters the oxidation state of both PANI and reduced graphene oxide. Among the tested substrates, polyethylene terephthalate (PET) exhibited the highest conductivity of 1.486 S/cm, which is attributed to an optimal coating thickness and uniform particle distribution.

Keywords: Conductive inks; Copper nanocomposite; CuNP-rGO-PANI; Graphene; Sensors

#### 1. Introduction

The advancement of nanomaterial-based sensor technology has become a significant area of interest in functional materials research, primarily due to the need for more efficient, flexible, and integrated sensor devices with printed electronic systems. In this context, graphene-based nanocomposites, such as reduced graphene oxide (rGO), have garnered considerable attention due to their exceptional electrical, thermal, and mechanical properties. Nevertheless, structural

<sup>&</sup>lt;sup>1</sup>Department of Agroindustrial Technology, Faculty of Agricultural Engineering and Technology, IPB University, Bogor 16680, Indonesia

<sup>&</sup>lt;sup>2</sup>Department of Industrial Engineering, Faculty of Creative Industries, Universitas Teknologi Bandung, Bandung 40235, Indonesia

<sup>\*</sup>Corresponding author: endangwarsiki@apps.ipb.ac.id, Tel.: +612518621974

This work was supported by the (1) Pusat Pembiayaan dan Asesmen Pendidikan Tinggi (Center for Higher Education Funding and Assessment)-PPAPT Ministry of Higher Education, Science, and Technology of Republic Indonesia, and (2) Education Fund Management Institution (LPDP), Ministry of Finance Indonesia. Fund Project Number: 1985/J5.2.3./BPI.06/10/2021.

modification is necessary to enhance the functionality of these materials by incorporating alternative conductive materials, such as metal nanoparticles (MNPs) and conductive polymers.

Nanocomposites represent a significant advancement in materials science, offering the unique ability to integrate the exceptional attributes of diverse materials into a unified and synergistic system. In recent years, various conductive materials have been developed for use in printed electronics. However, some inherent limitations restrict their application. For instance, polymerbased materials exhibit poor conductivity, while pure metal materials, including Au, Ag, Pt, and Cu (Park et al. 2007; Nur et al. 2002), demonstrate excellent conductivity but are prohibitively expensive for mass production due to their tendency to oxidize and exhibit poor sensitivity (Junervin et al., 2020). Carbon-based nanomaterials, including carbon-based nanofibers, activated carbon, and graphene, have been shown to exhibit optimized conductivity, a large surface area, and high anticorrosion ability (Trisnadewi et al., 2023; Murdiya et al., 2022; Gao, 2017; Qiu et al. 2017; Mohanapriya et al., 2016; Wang et al., 2016; Filip et al., 2015; Li et al. 2015). Graphene possesses distinctive properties, including a high surface area, high chemical stability, rapid electron transfer kinetics, and exceptional electrocatalytic properties (Hardi and Rahman, 2020; Kusrini et al., 2019; Xu et al., 2014). Because of these properties, graphene is frequently employed in synthesizing nanocomposites for sensing applications. To obtain the maximum physical and chemical characteristics, graphene must be subjected to a reduction process to produce rGO. Reduced graphene oxide (rGO) exhibits high electrical conductivity and a large surface area, facilitating efficient charge transfer and analyte (Fajarani et al., 2024; Yao, 2022; Bhangoji et al., 2021). However, the primary disadvantage of rGO is its tendency to aggregate and revert to a graphite form (Kumar et al., 2018). One actantial solution to this challenge is to synthesize graphene with various noble metals to create layered nanocomposites that enhance electrochemical processes (Mooss et al., 2017; Pandey and Qureshi, 2017; Li et al., 2017; Kalambate et al., 2015; Shahriary et al., 2015).

Metal-based nanocomposites, such as copper (CuNP) nanoparticles combined with rGO and polyaniline, have emerged as promising candidate materials for this application. The combination of the high conductivity properties of metals with the flexibility and chemical stability of rGO and PANI is anticipated to result in the creation of materials with optimal performance as essential elements in chipless RFID.

CuNPs offer high electrical conductivity at a low cost, are abundant, possess antimicrobial properties, and demonstrate significant electrochemical activity. Moreover, they can be readily synthesized in various nanoscale forms. Copper is receiving heightened interest because of its actantial use in sensors, its effectiveness in electrochromic coatings, and its potential use in superconductors (Nugrahaningtyas et al., 2025; Wu et al., 2017; Dobrovolný et al., 2016; Mousavi-Kamazani et al., 2016; Martinez-Lombardia et al., 2014; Reddy et al., 2014).

PANI is a conductive polymer that, when doped, enhances the overall electrical conductivity of the composite. PANI also provides flexibility and processability, which, when coupled with rGO and nanoparticles, results in composites with an optimal balance of conductivity, strength, and stability (Petrovski et al., 2017; Li et al., 2014; Liu et al., 2014).

CuNP/rGO/PANI nanocomposites offer potential advantages, such as excellent electrical conductivity, outstanding thermal stability, high mechanical strength, and enhanced catalytic or antimicrobial properties, compared to sensors based on metal oxide materials or carbon nanotubes, which have been widely used commercially (Shishir et al., 2024). This combination makes them highly suitable for applications in sensors, energy storage devices, coatings, and biomedical fields, where the composite's synergistic performance is crucial. This is because rGO provides sunport sites for CuNPs, preventing aggregation and improving their stability. Combining CuNPs, rGO, and PANI creates a percolation network for efficient charge transport. Additionally, the PANI polymer matrix maintains flexibility, while rGO enhances durability, thereby preventing degradation.

Additionally, CuNP-rGO-PANI nanocomposites demonstrate considerable actantial for incorporation into active and intelligent packaging technologies. In the context of active packaging,

CuNP has been demonstrated to possess antibacterial properties that can inhibit the growth of microorganisms, thereby extending the shelf life of the product. The potential of chitosan as a biomaterial for ethylene-absorbing active packaging has been investigated in a related field (Warsiki, 2018). Conversely, the conductive and flexible properties of CuNP-rGO-PANI facilitate the printing of sensors on the packaging surface, which can detect alterations in temperature, humidity, or product quality in real-time, thus enabling the development of innovative packaging. Integrating sensors into the packaging of agro-industrial products offers consumers several significant advantages, including freshness and quality assurance. Furthermore, it allows the retail industry to efficiently manage stock and verify product authenticity (Wisudawaty et al., 2024).

Although various synthesis methods, such as sol-gel, hydrothermal, and chemical vapor deposition, have been developed, challenges remain in optimizing the nanocomposite composition ratio and printing techniques to produce high-performance sensors. For instance, different synthesis methods can influence the electrical conductivity and stability of the sensor, whereas printing techniques, such as screen printing, can affect the print pattern and sensor reproducibility. The success of this application depends on the development of an ink formulation with optimal viscosity and high conductivity. Advancements in CuNP-rGO-PANI nanocomposite-based inks present a significant challenge, requiring a comprehensive scientific approach encompassing synthesis, characterization, and material performance evaluation.

This study offers a more controlled synthesis method by varying reaction conditions and optimizing reduction techniques to achieve a more uniform distribution of CuNPs within the rGO-PANI matrix. Additionally, it focuses on optimizing printing techniques, particularly by evaluating the effectiveness of screen printing on flexible substrates such as PET, glass, and photo paper, which has been rarely discussed in previous studies.

This research aims to develop and characterize CuNP-rGO-PANI nanocomposites, utilize the nanocomposites as conductive inks, and evaluate their conductivity properties for printed sensor technology. Therefore, this research is expected to contribute to the development of more effective, efficient, and sustainable nanocomposite-based printed sensors.

#### 2. Methods

#### 2.1 Synthesis of Graphene Oxide (GO)

GO was synthesized using the modified Hummers method, as described by Liu et al. (2014). 6 g of graphite powder was dissolved in 130 mL of concentrated sulfuric acid (98%  $H_2SO_4$ ). Subsequently, 4 g of NaNO<sub>3</sub> were added and stirred for 4 h (temperature <20°C) by placing the mixture in an ice bath. After 2 h of stirring, 8 g of KMnO<sub>4</sub> was added to the solution gradually, after which homogenization was conducted for a further 2 h at 35°C. Subsequently, 200 mL of distilled water was gradually incorporated and homogenized for 1 h. Subsequently, 20 mL of  $H_2O_2$  (30%) was added to remove any residual KMnO<sub>4</sub>.

Subsequently, the mixture was centrifuged, and 80 mL of HCl was introduced to facilitate the elimination of any residual metal impurities. Subsequently, the pH was neutralized through leaching, and the residual  $SO_4^{2-}$  ions were minimized. Once a neutral pH was reached, the mixture was dried for 12 hours at  $110^{\circ}$ C for 12 h. Subsequently, the dried graphene oxide (GO) was exfoliated to create graphene oxide sheets. GO (40 mg) was combined with distilled water (40 mL), stirred for 1 h to form a homogeneous solution, and subjected to ultrasonication for 120 min. The application of ultrasonic waves resulted in the peeling of graphite oxide into GO.

#### 2.2. Reduced graphene oxide (rGO)

The graphene oxide (GO) obtained from the ultrasonication process was subjected to a chemical reduction process using sodium borohydride (NaBH<sub>4</sub>). The reduction process is conducted by introducing NaBH<sub>4</sub> to the graphene oxide suspension in a ratio of 9:7 (Sharma et al., 2017), while vigorously stirring for 10 min. Subsequently, the solution was placed in an autoclave at 200°C for 5 h (Kumar et al., 2018). Following the reduction process, the rGO was subjected to a pH

neutralization procedure involving a washing step with running water. Subsequently, the material was transformed into a powder form by drying at 110°C.

## 2.3. Synthesis of CuNP-rGO-PANI Nanocomposites

Aniline polymerization was employed in situ to synthesize the CuNP-rGO-PANI nanocomposites. The process involved the preparation of 3 distinct solutions. Solution A: rGO (200 mg) was dissolved in 200 mL of water, and the resulting solution was subjected to sonication for 120 min. Solution B: Copper sulfate pentahydrate (CuSO<sub>4</sub>·5H<sub>2</sub>O) was dissolved in distilled water and stirred for 20 min to create a 0.01 M solution. A solution of 0.02 M ascorbic acid was prepared in distilled water. Subsequently, the copper sulfate solution was added to the ascorbic acid solution, and the mixture was stirred continuously. To adjust the pH, 1 M NaOH was added to distilled water. After a 30-min stirring period, 0.1 M NaBH<sub>4</sub> in distilled water was gradually introduced with continuous stirring. After 15 min, the initial blue mixture underwent a color change, becoming reddish-brown. The researchers prepared Solution C by dissolving 2 mL of aniline in 60 mL of distilled water, then adding 0.5 mL of concentrated HCl and homogenizing for 30 min.

The CuNP-rGO-PANI nanocomposite was prepared: Solutions A and B and stirring them for 1 h. Then, Solution C was added and stirred for another 20 minutes. Subsequently, 40 mL of an aqueous solution containing 1 g of APS was gradually added. The mixture was homogenized and polymerized for 12 h. The precipitate obtained was washed under running water. The nanocomposite in powder form was obtained by drying the precipitate at 70°C.

#### 2.4. Sample Characterization

Various analytical techniques were employed to characterize the processed samples. Raman spectroscopy is a technique that is used to identify molecules, analyze chemical structures, and investigate molecular interactions within a given sample. This method is based on inelastic light scattering, also known as Raman scattering, in which the light incident on a sample undergoes a frequency shift due to interaction with the molecular vibrations of the sample. The morphology of the sample was examined using a scanning electron microscope (SEM), and any complex groups were identified using a Fourier transform infrared (FTIR) spectrometer.

#### 2.5. Preparation of Conductive Ink and Sensor Printing

The conductive ink was prepared by combining a conductive material, specifically a CuNP-rGO-PANI nanocomposite, with an epoxy resin and dispersing the mixture in distilled water and ethanol. This resulted in a paste-like ink, which was subsequently used in the fabrication of sensors. The sensor was printed using the screen printing method with a T90 mesh screen. The patterns in the form of lines with dimensions of  $1 \times 2$  cm were printed on paper and transferred to a screen previously coated with emulsion. Subsequently, the screen was subjected to solar drying for approximately 20 seconds and rinsed with water until the requisite pattern was formed. The conductive ink was then applied to the screen and printed on Polyethylene Terephthalate (PET) (Liu et al., 2021), glass, and paper (Figure 1). Once the printing process is complete, the printed material must be cured in an oven at  $100^{\circ}$ C for 12 minutes.

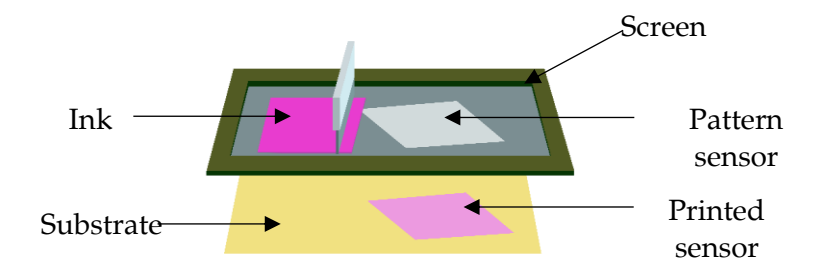


Figure 1 Screen printing method

#### 2.6. Sensor Characterization

The previously manufactured film-shaped sensor was subjected to electrical conductivity measurement via the 4-point probe method, employing a multimeter and a 12 V current source. Equations 1 and 2 are used to calculate the electrical conductivity (Istuk et al., 2023):

$$\rho = \frac{V}{I} + \frac{d}{s} + C' \tag{1}$$

$$\sigma = \frac{1}{\rho} \tag{2}$$

Description:

 $\rho$  = resistivity ( $\Omega$ )

V = electric actantial difference (V)

I = electric current (A)

d = sample surface width (cm)

s = distance between the probes (cm)

C' = correction factor

 $\sigma$  = electrical conductivity (S/cm)

#### 3. Results and Discussion

## 3.1. Results of the Synthesis of CuNP-rGO-PANI Nanocomposites

Graphene oxide is produced from graphite base material through the Hummers oxidation method (Liu et al., 2014). The oxidation process entails the use of potent acids, which facilitate the disruption of intercarbon bonds and the spacing of graphene sheets. Subsequently, exfoliation is conducted via ultrasonication, resulting in complete disruption of the inter-sheet bonds. Specific oxide groups must be eliminated through a reduction process to enhance the chemical and physical attributes of graphene, which can be accomplished either through chemical means or hydrothermal methods, resulting in reduced rGO. Nevertheless, the primary disadvantage of rGO is its proclivity to agglomerate and revert to the graphitic form (Kumar et al., 2018). Incorporating copper (Cu) nanoparticles via aniline in situ polymerization is designed to function as nanoscale spacers, increasing the distance between graphene sheets (Tien et al., 2011) and thus preventing their aggregation. Figure 2 shows the synthesis process of the CuNP-rGO-PANI nanocomposites.

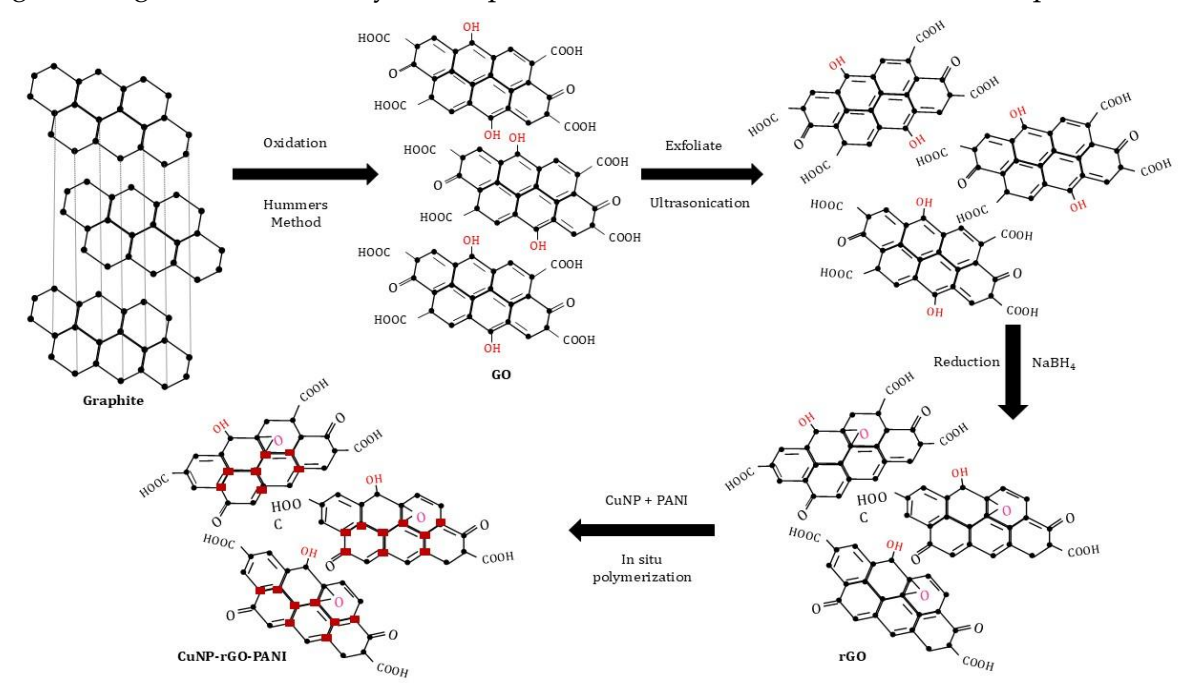


Figure 2 Synthesis process of CuNP-rGO-PANI nanocomposites

The CuNP-rGO-PANI nanocomposite, which was synthesized from copper nanoparticles via the chemical reduction of CuSO<sub>4</sub> using NaBH<sub>4</sub> as the reducing agent, exhibited a brownish-red coloration. This coloration indicates the successful formation of copper NPs during the reduction process. Similarly, previous research has employed NaBH<sub>4</sub> as a reducing agent to synthesize copper particles with sizes ranging from 15 to 50 nm. The brownish-red color result is also obtained from the studies of Amjad et al. (2021) and Choi et al. (2016), who also employed NaBH<sub>4</sub> as the reductant. The following mechanism can elucidate the chemical reaction between CuSO<sub>4</sub> and NaBH<sub>4</sub>:

$$CuSO_4 + 2NaBH_4 + 6H_2O \rightarrow Cu(s) + 2B(OH)_3 + 2NaOH + 4H_2(g)$$
 (3)

The combination of colloidal CuNPs and rGO resulted in the deposition of CuNPs on graphene sheets (red rectangles in Figure 2). Aniline functions as a stabilizing agent for copper nanoparticles, forming an aniline-Cu complex through in situ polymerization. A change in the color of the mixed solution to a greenish-black hue indicates the occurrence of the polymerization process.

To illustrate the interaction of all components in the formation of the CuNPs-rGO-PANI nanocomposite, the process begins with the reduction of graphene oxide into reduced graphene oxide (rGO) using NaBH<sub>4</sub>, which leads to structural changes by removing oxygen functional groups. Next, CuNPs are formed through the reduction of  $Cu^{2^+}$  ions, with their interaction with rGO occurring via  $\pi$ - $\pi$  stacking or electrostatic forces. Subsequently, polyaniline (PANI) is synthesized through the oxidative polymerization of aniline monomers on the rGO-CuNPs surface, where PANI interacts with CuNPs and rGO via hydrogen bonding or electrostatic attraction. Finally, the well-dispersed CuNPs on rGO combined with the PANI matrix create a conductive network, forming the CuNPs-rGO-PANI nanocomposite.

In the formation of CuNP-rGO-PANI nanocomposites, several crucial interactions occur among the CuNPs, rGO, and PANI components, which determine the structural, morphological, and functional properties of the resulting nanocomposites. Interaction of CuNPs with rGO: In situ CuNPs can interact with the functional oxygen groups on the rGO surface through electrostatic forces. Functional groups such as carbonyl (-C=O) and hydroxyl (-OH) on rGO serve as nucleation sites for CuNP growth. CuNPs can adsorb onto the surface of rGO via  $\pi$ - $\pi$  interactions between the free electrons on Cu metal and the aromatic structure of rGO. Additionally, rGO prevents CuNP agglomeration by providing a large surface area that sunport even nanoparticle dispersion (Pegu et al., 2023).

Interaction of CuNPs with PANI: CuNPs interact with the amine (-NH) and imine (=N) groups within the PANI polymer chain. CuNPs act as doping agents for PANI, enhancing conductivity by modifying the electronic structure of the polymer. The functional groups in PANI can form complexes with copper ions during synthesis, thereby improving the stability of CuNPs. The aromatic structure of PANI enables  $\pi$ - $\pi$  interactions with rGO, thereby enhancing electron transfer. Amine (-NH) and hydroxyl (-OH) groups in PANI can interact with functional oxygen groups on rGO through hydrogen bonding. The combination of rGO and PANI improves the conductivity of the nanocomposite, as rGO serves as a rapid electron transfer pathway, while PANI provides mechanical flexibility.

The CuNP-rGO-PANI nanocomposite is formed through a combination of electrostatic, covalent, and  $\pi$ - $\pi$  stacking interactions among its components. The presence of rGO sunport CuNP dispersibility and enhances the conductivity of the nanocomposite, while PANI provides structural stability and flexibility. These synergistic interactions make CuNP-rGO-PANI a promising candidate for sensor applications and conductive inks (Pegu et al., 2023).

#### 3.2. Results of Raman Spectroscopy Characterization

Raman spectroscopy offers insights into the extent of rGO reduction and the intermolecular interactions between different components (Sonawane et al., 2019). As illustrated in Figure 3(a), two distinct peaks are discernible at 1346.80 cm<sup>-1</sup> and 1597.81 cm<sup>-1</sup> wavenumbers. These are designated as the D (defect) and G (graphitic) peaks, respectively, and serve as carbon marker spectra in Raman

spectroscopy. Characterization results indicate a ratio of 1.2 between the intensity of the ID and IG peaks. The elevated intensity of the D peak and the ID/IG ratio confirm the formation of a defective rGO structure. The defects are primarily attributable to the chemical reduction process, which removes oxide groups, including C=O (carbonyl), O-H (hydroxyl), and C-OH (carboxyl), thereby disrupting the  $\pi$ -conjugated network in the graphene structure. Some of the remaining oxide groups may also contribute to the formation of structural defects (Chadha et al., 2021).

As illustrated in Figure 3(b), the peaks emerge at 1340.61 cm<sup>-1</sup> and 1550.27 cm<sup>-1</sup>, accompanied by an increase in the intensity of the D peak, culminating in an ID/IG ratio of 1.28. The increase in the ratio from rGO (1.2) to CuNP-rGO-PANI (1.28) may indicate the presence of structural defects, which could enhance the sensitivity of the sensor. If an interaction occurs between CuNPs and rGO-PANI, it indicates the potential for improved conductivity and sensing properties. This enhancement is attributed to the unique electrical characteristics of metal nanoparticles, which can significantly boost the electrochemical response and efficiency of sensors for detecting various analytes when combined with conducting polymers (Shen et al., 2021).

The results of Raman spectroscopy indicate that the incorporation of copper nanoparticles (CuNPs) increases the ID/IG ratio, indicating an enhancement in the prevalence of structural defects in rGO. This is attributed to the interaction between the nanoparticles and the rGO matrix and the thermal processes that occur during the synthesis phase. The thermal process employed during nanocomposites synthesis also affects the structure of rGO and metal nanoparticles, thereby contributing to the observed structural defects.

Several key factors cause the significant changes in the Raman spectra after combining rGO with PANI and Cu. The electronic interaction between rGO, PANI, and Cu alters the electron distribution, affecting the vibrational modes of carbon bonds in rGO. The presence of CuNPs also contributes through charge transfer, which can reduce the intensity of the D and G peaks in the Raman spectrum. Additionally, the rGO structure undergoes modifications due to increased defects or disorder when integrated with PANI and Cu, potentially increasing the ID/IG ratio. The optical shielding effect of CuNPs and PANI also plays a role in reducing the Raman spectrum intensity, as both can absorb or scatter the excitation laser light (Jezzini et al., 2024; Saini et al., 2024).

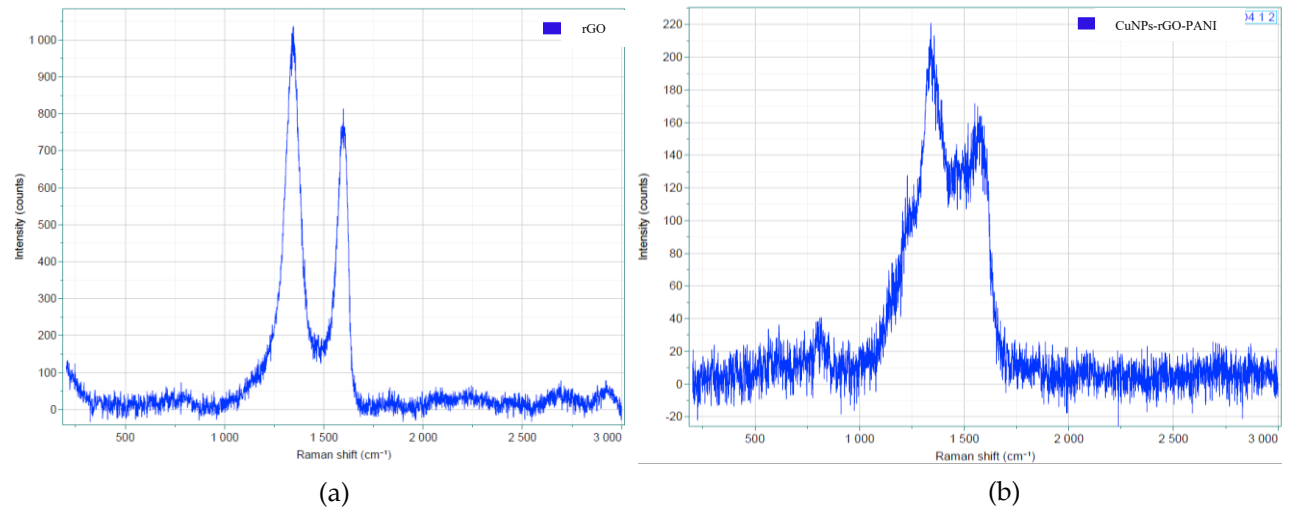


Figure 3 Raman spectroscopy results of (a) rGO and (b) CuNPs-rGO-PANI

#### 3.3. SEM Characterization Results

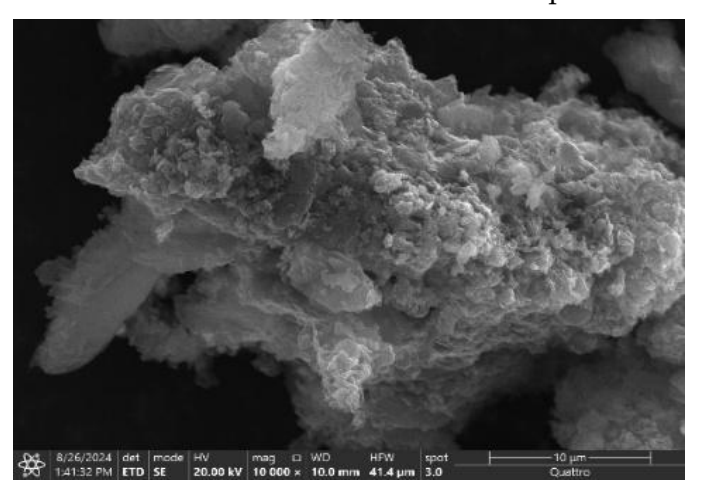
The surface area morphology of the graphene-based nanocomposites was examined using scanning electron microscopy (SEM). A scanning electron microscopy (SEM) provides a relatively low-resolution overview of the composite's surface morphology, revealing the general distribution of copper nanoparticles (CuNPs), reduced graphene oxide (rGO) sheets, and polyaniline (PANI) structures (Darwish et al., 2019). Electron microscopy images illustrate the structure of rGO as

graphene sheets exfoliated by ultrasonication. Similar findings were reported by Gul et al. (2023) and Sharma et al. (2017), who employed the Hummers method for synthesis (Liu et al., 2014). Meanwhile, the morphology of the nanocomposites, comprising Cu and PANI particles of varying sizes and shapes, dispersed and adhered to the rGO surface. Microscopic examination reveals that the particles are irregularly shaped and uniformly distributed. Surface pores result in a significantly clustered mesostructure, facilitating the dispersion of metal ions into the nanocomposite matrix (Salamani et al., 2018).

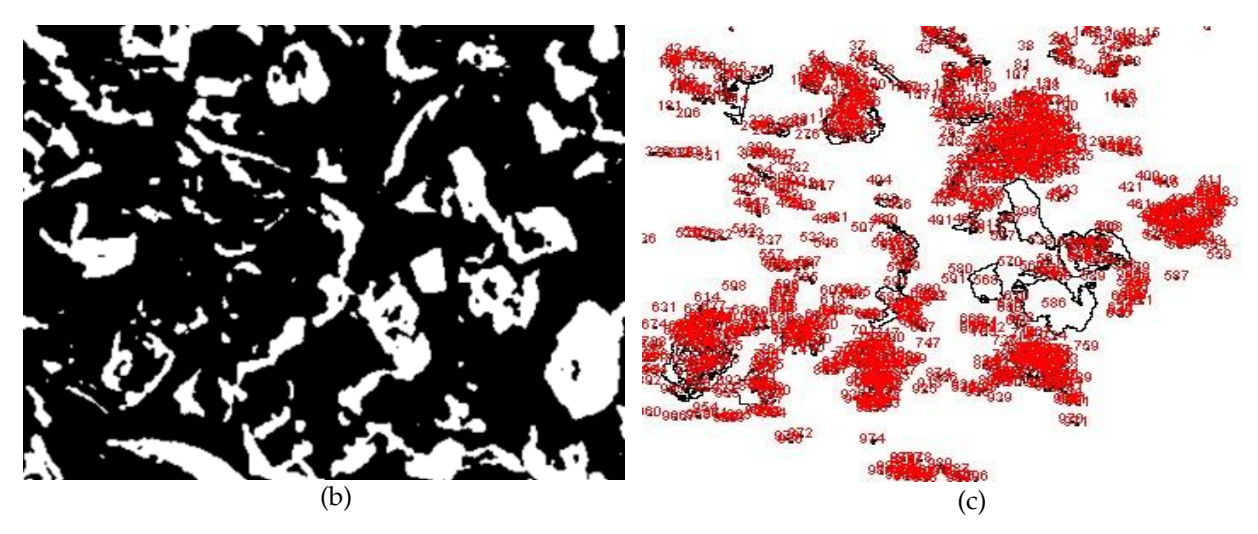
A semi-quantitative calculation of the particle size distribution was performed based on the obtained SEM image using ImageJ software for image processing (Fritz et al., 2024; Sasri et al., 2018). The initial step involves calibrating the digital image by setting the appropriate scale. Next, the SEM digital images are processed using the Threshold function to enhance the distinction between the object and its background. The analysis is then performed using the Analyze > Analyze Particles tool, which provides data on the total area of all identified particles. Assuming that the particles are spherical, their diameters can be estimated based on the calculated average area. The particle size distribution was calculated using the ImageJ software, as illustrated in the following example.

Figure 4 illustrates the outcomes of image processing conducted with the ImageJ software, which was employed to ascertain the PSD. Figure 4a shows the SEM images of CuNP-rGO-PANI nanocomposites that have undergone image calibration. The threshold results, which differentiate the object in question from the background (Figure 4b), are presented below. Figure 4c illustrates the outline results, which display the defined area data. The following section presents the particle size distribution with the data obtained through ImageJ software.

The particle size distribution obtained through image analysis using ImageJ software is presented in Figure 5 and Table 1. The CuNP-rGO-PANI nanocomposite particles exhibit an average diameter of 11.48 nm, ranging from 7.67 to 99.68 nm. This is consistent with the typical nanoscale range of 1-100 nm, as previously reported by (Mekuye and Abera, 2023; Joudeh and Linke, 2022). In conclusion, the SEM analysis provided a comprehensive representation of the morphology and particle size distribution, indicating that the synthesis method effectively yielded nanocomposites with an optimal nanosize and considerable actantial for RFID chipless sensor applications.



**Figure 4** a. SEM characterization results of CuNP-GO-PANI at ×20000 magnification, b. Treshold results of CuNP-rGO-PANI in the ImageJ software, c. Outline of the results of CuNP-rGO-PANI in ImageJ software



**Figure 4** a. SEM characterization results of CuNP-GO-PANI at ×20000 magnification, b. Treshold results of CuNP-rGO-PANI in the ImageJ software, c. Outline of the results of CuNP-rGO-PANI in ImageJ software (Cont.)

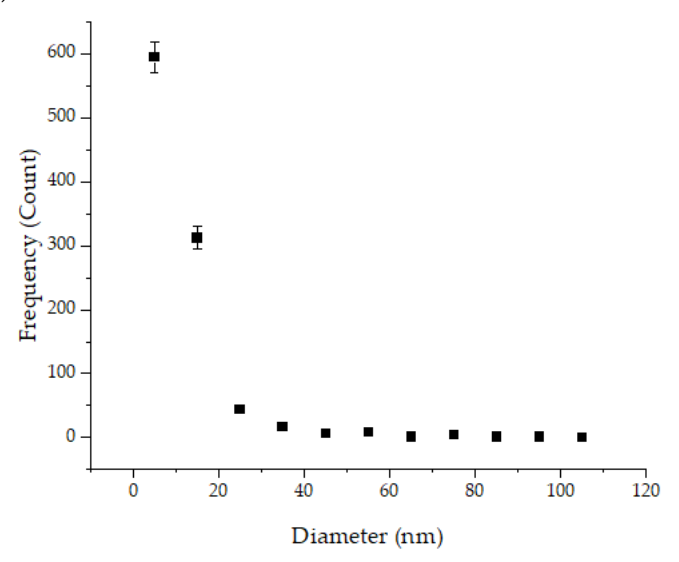


Figure 5 Particle size distribution of CuNP-rGO-PANI nanocomposites using ImageJ software

**Table 1** Results of particle size calculation

Nanocomposites	Average area (nm²)	Mean Diameter (nm)	Smallest diameter (nm)	Largest diameter (nm)
CuNP-rGO-PANI	667.23	11.48	7.67	99.68

## 3.4. FTIR Spectrophotometer Characterization

FTIR spectroscopy was used to ascertain the chemical functionalities of the CuNP-rGO-PANI nanocomposites (Valan et al., 2022). This analysis is based on the detection of transmittance peaks in infrared spectra associated with specific chemical bond vibrations in the material. By analyzing these spectra, it is possible to identify the formed functional groups and establish a link between them and the material's structure. Fourier transform infrared spectroscopy is a widely employed method for elucidating the chemical alterations and interactions occurring between the constituents of a nanocomposite.

Figure 6(a) shows the FTIR characterization results of rGO, which reveal the presence of the leading functional group of rGO, C=C, at a wavenumber of 1569 cm<sup>-1</sup>. This peak is typically associated with sp<sup>2</sup> hybridized carbon atoms and C-C stretching vibrations within the graphene

lattice. This peak indicates conjugated double bonds, which constitute the rGO structure's backbone. Many oxygen groups are removed during the reduction process. The C=C functional group represents the fundamental structure of rGO, comprising hexagonal carbon double bonds. It contributes to the strength and electrical conductivity of the material due to its high bond energy. These findings are consistent with those reported by Gul et al. (2023), Mallakpour and Hussain (2021), and Kumar et al. (2018) on rGO and graphene materials. Additionally, another absorption peak appears at 3579 cm<sup>-1</sup>, indicating an O-H functional group, which suggests the presence of water in the compound.

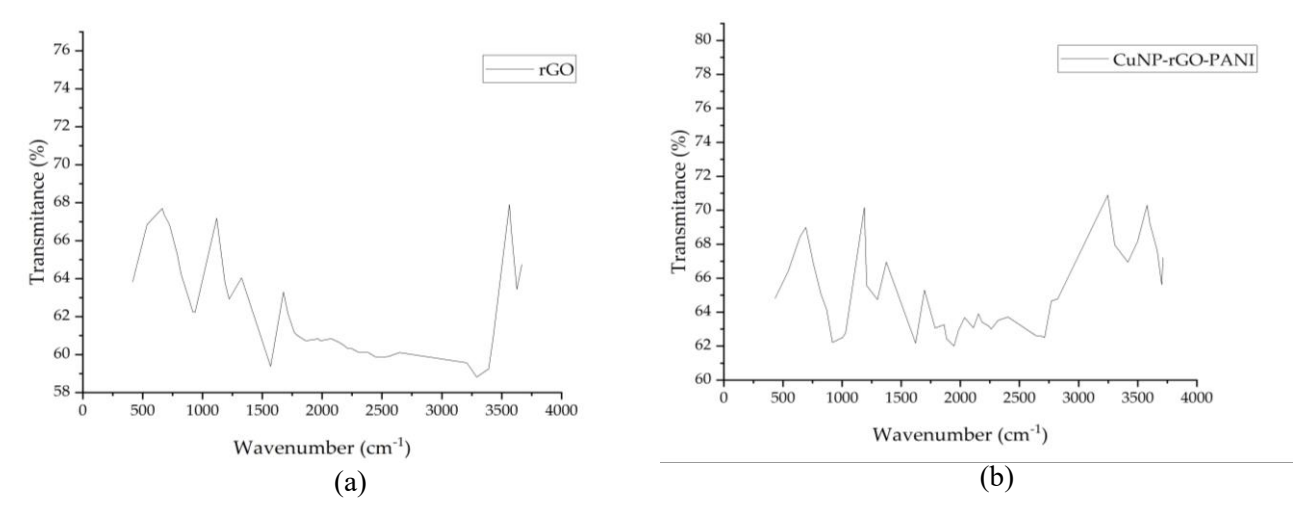


Figure 6 FTIR spectra of (a) rGO and (c) CuNP-rGO-PANI

The FTIR characterization of the CuNP-rGO-PANI nanocomposite revealed an absorption peak at 1300 cm<sup>-1</sup> (Figure 6(b)). The observed peak indicates C-O bonds derived from carboxyl or phenolic groups in rGO that interact with PANI. Furthermore, it suggests the existence of interactions or binding between polyaniline and rGO, as well as between rGO and CuNP. Furthermore, an additional absorption peak was identified at 1622 cm<sup>-1</sup>, frequently associated with C-C vibrations. This confirms the presence of an aromatic PANI structure. This results in the retention of the polyaniline structure in the composite, with interactions that affect the electronic structure of polyaniline, though not to the extent of destruction. Furthermore, the incorporation of CuNPs has been observed to affect the oxidation state of PANI and the reduction of graphene oxide, which in turn gives rise to changes in peak intensity and position in the Fourier transform infrared (FTIR) spectrum (Singh et al., 2022). Another absorption peak appears at 3416 cm<sup>-1</sup>, indicating the N-H group in aniline.

#### 3.5. Conductive Ink Formulation and Sensor Printing

The sensor printing process, conducted using the screen printing method, yielded three sensors with distinct substrate types. Table 2 shows the thickness of each sensor after the curing process. The sensor layer thickness on PET plastic, photo paper, and glass substrates exhibits notable discrepancies that influence the functionality of CuNP-rGO-PANI-based conductive ink sensors. The distinctive attributes of each substrate influence the sensors' flexibility, mechanical resistance, and sensitivity, which are essential for their functionality. The ink layer thickness after curing on PET plastic substrates is 0.27 mm, providing an optimal balance between flexibility and mechanical resistance, which is crucial for applications where durability is a prerequisite (Lepak-Kuc et al., 2022). The ink layer on photo paper is of a lesser thickness, measuring approximately 0.19 mm after curing. This increases sensitivity but reduces mechanical resistance, which makes the sensor more susceptible to damage (Brathwaite et al., 2023).

In contrast, the ink is less likely to permeate on glass, resulting in a thicker layer (approximately 0.31 mm after curing), which offers enhanced structural stability but may compromise flexibility,

which is critical for specific applications (Yi et al., 2021). The coating thickness generally depends on the substrate type and the molding technique employed. While thinner layers enhance sensitivity, they may diminish durability, underscoring a trade-off in substrate-based sensor design. Conversely, a thicker coating on a more rigid substrate may enhance stability but may constrain flexibility, underscoring the need for meticulous deliberation in sensor applications.

Table 2 Sensor printing results based on the substrate used

Substrate	Flat thickness(mm)	
PET	0.27	
Glass	0.31	
Photo paper	0.19	

### 3.6. Sensor electrical conductivity measurement results

Direct current conductivity measurements are used to measure the overall electrical conductivity of the nanocomposite. This measurement indicates the ease with which charge carriers can traverse a material under a constant electric field. The electrical conductivity of the sensor was determined by applying the four-point probe method, with the resulting data subsequently calculated in accordance with the Smits equation (Istuk et al., 2023). Table 3 presents the parameters of the electrical conductivity measurement results of the sensor.

Table 3 Measurement results of the resistivity and electrical conductivity of the sensor

Substrate	Resistivity (Ωcm)	Electrical conductivity (S/cm)
PET	673.14 x 10 <sup>-3</sup>	1.49
Glass	$821.52 \times 10^{-3}$	1.22
Photo paper	$943.75 \times 10^{-3}$	1.06

The thickness of the ink layer, the distribution of conductive particles (CuNP and rGO), and the substrate utilized significantly affect the conductivity of the CuNP-rGO-PANI-based conductive ink sensor. The resistivity of the CuNP-rGO-PANI-based conductive ink sensor on a PET plastic substrate is lower ( $673.14 \times 10^{-3} \Omega cm$ ), which is inversely proportional to the higher electrical conductivity of 1.486 S/cm. This is due to the optimal ink layer thickness and relatively smooth surface of PET, allowing for a more even distribution of CuNPs and rGO nanoparticles, forming effective conduction pathways, and enhancing electron transport (Henley et al., 2015). On photo paper, despite the thinner ink layer, the ink's uneven distribution and the paper's absorbent nature result in an increased resistivity (943.75 x  $10^{-3} \Omega cm$ ), which in turn leads to a reduction in conductivity. Conversely, glass substrates exhibit a lower conductivity of 1.0596 S/cm compared to PET due to the greater thickness of the ink layer, which impedes electron transport. However, glass displays superior structural stability (Henley et al., 2015). PET generally provides optimal conductivity, whereas photographic paper and glass exhibit decreased conductivity due to suboptimal coating thickness and uneven particle distribution.

The resistivity value is calculated based on the thickness measurement of the printed pattern on the substrate. The sensor, printed on photo paper, exhibited a high resistivity value of 943.75 x 10<sup>-3</sup>. The resistivity value obtained on photo paper is superior to that obtained on glass and PET substrates. Multiple studies have demonstrated that glossy photo paper (Epson) contains a surface coated with chloride ions. These ions migrate to the copper film during copper dispersion deposition and fluid vehicle absorption, promoting the deagglomeration of copper nanoparticles and assisting the sintering process (Vaseem et al., 2016; Magdassi et al., 2010). The resistivity values on PET substrates are superior to those printed on other substrates, as a lower resistivity of an ink correlates with enhanced conductivity (Fernandes et al., 2020; Magdassi et al., 2010). Nevertheless, the higher copper nanoparticle content (30 wt%) employed can be attributed to the relatively low resistivity value.

#### 4. Conclusions

CuNP-rGO-PANI nanocomposites have considerable actantial for use in various printed sensor applications. The structure and characteristics of the nanocomposite materials are significantly influenced by the inclusion of copper nanoparticles. The Raman spectroscopy results demonstrated that the incorporation of Cu nanoparticles elevated the ID/IG ratio, indicating an augmentation in structural defects in rGO due to the interaction between nanoparticles and the rGO matrix and thermal processes that occurred during synthesis. The particle size of the CuNP-rGO-PANI nanocomposite was determined to be 11.48 nm on average through SEM analysis. FTIR characterization demonstrated the interaction between polyaniline (PANI), reduced graphene oxide (rGO), and copper nanoparticles (CuNP), which affected the electronic structure of PANI without significantly damaging it. Furthermore, the addition of CuNPs alters the oxidation state of PANI and reduces graphene oxide, as evidenced by shifts in the intensity and position of the FTIR peaks. The conductivity of the CuNP-rGO-PANI-based conductive ink sensor depends on the ink layer thickness, conductive particle distribution, and substrate type. The PET plastic substrate exhibited the highest conductivity of 1.486 S/cm, which was attributed to the optimal coating thickness and uniform particle distribution. In contrast, the conductivity of the photographic paper and glass substrates was lower, which can be attributed to suboptimal coating thickness and uneven particle distribution. The conductivity of the sensor is primarily determined by the thickness of the ink layer and the surface properties of the substrate.

## Acknowledgements

The author would like to thank the following institutions for granting this doctoral scholarship at BPI (Beasiswa Pendidikan Indonesia) with the ID number 202101122325, and for supporting this research: (1) Pusat Pembiayaan dan Asesmen Pendidikan Tinggi (Center for Higher Education Funding and Assessment)-PPAPT Ministry of Higher Education, Science, and Technology of Republic Indonesia, and (2) Lembaga Pengelola Dana Pendidikan (Education Fund Management Institution)-LPDP, Ministry of Finance Indonesia. Fund Project Number: 1985/J5.2.3./BPI.06/10/2021.

## **Author Contributions**

Priska Wisudawaty: Writing-original draft, review & editing. Endang Warsiki: Review, editing, and supervision. Sugiarto: Review and supervision. Taufik Djatna: Review, editing, and supervision.

#### Conflict of Interest

The authors declare no conflicts of interest.

#### References

Amjad, R, Mubeen, B, Ali, SS, Imam, SS, Alshehri, S, Ghoneim, MM, Alzarea, SI, Rasool, R, Ullah, I, Nadeem, MS & Kazmi, I 2021, 'Green synthesis and characterization of copper nanoparticles using *fortunella margarita* leaves', *Polymers*, vol. 13, no. 24, article 4364, <a href="https://doi.org/10.3390/polym13244364">https://doi.org/10.3390/polym13244364</a>

Bhangoji, JC, Sahoo, S, Satpati, AK & Shendage, SS 2021, 'Facile and green synthesis of silver nanoparticle-reduced graphene oxide composite and its application as nonenzymatic electrochemical sensor for hydrogen peroxide', *Current Chemistry Letters*, vol. 10, no. 3, pp. 295-308, <a href="https://doi.org/10.5267/j.ccl.2021.3.002">https://doi.org/10.5267/j.ccl.2021.3.002</a>

Brathwaite, KG, Wyatt, QK, Atassi, A, Gregory, SA, Throm, E, Stalla, D, Yee, SK, Losego, MD & Young, MJ 2023, 'Effects of film thickness on electrochemical properties of nanoscale polyethylenedioxythiophene (PEDOT) thin films grown by oxidative molecular layer deposition (oMLD)', *Nanoscale*, vol. 15, no. 13, pp. 6187-6200, <a href="https://doi.org/10.1039/d3nr00708a">https://doi.org/10.1039/d3nr00708a</a>

Chadha, N, Sharma, R & Saini, P 2021, 'A new insight into the structural modulation of graphene oxide upon chemical reduction probed by Raman spectroscopy and X-ray diffraction', *Carbon Letters*, vol. 31, no. 6, pp. 1125-1131, <a href="https://doi.org/10.1007/s42823-021-00234-5">https://doi.org/10.1007/s42823-021-00234-5</a>

Choi, MW, Bae, MH & Ahn, J-H 2016, 'Synthesis of copper nanoparticles by a chemical reduction method', *Journal of Korean Powder Metallurgy Institute*, vol. 23, no. 3, pp. 228-234, https://doi.org/10.4150/kpmi.2016.23.3.228

Darwish, AG, Ghoneim, A, Hassaan, MY, Shehata, OS & Turky, GM 2019, 'Synthesis and characterization of polyaniline/Mn3O4/reduced graphene oxide nanocomposite', *Egyptian Journal of Chemistry*, vol. 62, pp. 251-265, <a href="https://doi.org/10.21608/ejchem.2019.13194.1821">https://doi.org/10.21608/ejchem.2019.13194.1821</a>

Dobrovolný, K, Ulbrich, P & Bartůněk, V 2016, 'Synthesis of ultrafine metallic copper nanocubes using ethanol-ionic liquid approach', *Journal of Cluster Science*, vol. 27, no. 6, pp. 1843-1847, <a href="https://doi.org/10.1007/s10876-016-1065-0">https://doi.org/10.1007/s10876-016-1065-0</a>

Fajarani, R, Rahman, SF, Pangesty, AI, Katili, PA, Park, DH & Basari 2024, 'Physical and chemical characterization of collagen/alginate/poly(vinyl alcohol) scaffold with the addition of multi-walled carbon nanotube, reduced graphene oxide, titanium dioxide, and zinc oxide materials', *International Journal of Technology*, vol. 15, no. 2, pp. 332-341, <a href="https://doi.org/10.14716/ijtech.v15i2.6693">https://doi.org/10.14716/ijtech.v15i2.6693</a>

Fernandes, IJ, Aroche, AF, Schuck, A, Lamberty, P, Peter, CR, Hasenkamp, W & Rocha, TLAC 2020, 'Silver nanoparticle conductive inks: Synthesis, characterization, and fabrication of inkjet-printed flexible electrodes', *Scientific Reports*, vol. 10, no. 1, article 8878, <a href="https://doi.org/10.1038/s41598-020-65698-3">https://doi.org/10.1038/s41598-020-65698-3</a>

Filip, J, Kasák, P & Tkac, J 2015, 'Graphene as signal amplifier for preparation of ultrasensitive electrochemical biosensors', *Chemical Papers*, vol. 69, no. 1, pp. 112-133, <a href="https://doi.org/10.1515/chempap-2015-0051">https://doi.org/10.1515/chempap-2015-0051</a>

Fritz, M, Deutsch, LF, Wijaya, KP, Götz, T & Fischer, CB 2024, 'An image-processing tool for size and shape analysis of manufactured irregular polyethylene microparticles', *Microplastics*, vol. 3, no. 1, pp. 124-146, <a href="https://doi.org/10.3390/microplastics3010008">https://doi.org/10.3390/microplastics3010008</a>

Gao, Y 2017, 'Graphene and polymer composites for supercapacitor applications: A review', *Nanoscale Research Letters*, vol. 12, no. 1, article 387, <a href="https://doi.org/10.1186/s11671-017-2150-5">https://doi.org/10.1186/s11671-017-2150-5</a>

Gul, W, Akbar Shah, SR, Khan, A, Ahmad, N, Ahmed, S, Ain, N, Mehmood, A, Salah, B, Ullah, SS & Khan, R 2023, 'Synthesis of graphene oxide (GO) and reduced graphene oxide (rGO) and their application as nanofillers to improve the physical and mechanical properties of medium density fiberboard', *Frontiers in Materials*, vol. 10, pp. 1-10, <a href="https://doi.org/10.3389/fmats.2023.1206918">https://doi.org/10.3389/fmats.2023.1206918</a>

Hardi, GW & Rahman, SF 2020, 'Amperometric detection of dopamine based on a graphene oxide/PEDOT:PSS composite electrode', *International Journal of Technology*, vol. 11, no. 5, pp. 974-983, <a href="https://doi.org/10.14716/jitech.v11i5.4323">https://doi.org/10.14716/jitech.v11i5.4323</a>

Henley, SJ, Kula, M, Brunton, AN, Chan, CWA, Dixon, R & Dunne, B 2015, 'Low-cost copper conductive grids for thin-film solar cells formed by screen printing and laser sintering', *In:* 2015 IEEE 42nd Photovoltaic Specialist Conference (PVSC), pp. 2-4, <a href="https://doi.org/10.1109/PVSC.2015.7356285">https://doi.org/10.1109/PVSC.2015.7356285</a>

Istuk, N, Benchakroun, H, Elahi, A, O'halloran, M, Matta, R, Moreau, D, O'connor, R & Dunne, E 2023, 'Reducing sensing volume confounding effects in conductivity measurements: The use of a miniaturised four-electrode probe', *In:* ICECOM 2023 - 24th International Conference on Applied Electromagnetics and Communications, <a href="https://doi.org/10.1109/ICECOM58258.2023.10367941">https://doi.org/10.1109/ICECOM58258.2023.10367941</a>

Jezzini, A, Davidson, A, Hamieh, T & Toufaily, J 2024, 'Exploring reduced graphene oxide sheets stabilized by Cu(II) and Cu(I) cations in ethanol', *Crystals*, vol. 14, no. 7, article 654, <a href="https://doi.org/10.3390/cryst14070654">https://doi.org/10.3390/cryst14070654</a>

Joudeh, N & Linke, D 2022, 'Nanoparticle classification, physicochemical properties, characterization, and applications: A comprehensive review for biologists', *Journal of Nanobiotechnology*, vol. 20, no. 1, pp. 1-29, https://doi.org/10.1186/s12951-022-01477-8

Junervin, Djatna, T & Fahma, F 2020, 'A synthesis of AgNP-rGO-PANI nanocomposite and its use in fabrication of chipless RFID sensor: Current research progress', *IOP Conference Series: Earth and Environmental Science*, vol. 472, no. 1, article 012027, <a href="https://doi.org/10.1088/1755-1315/472/1/012027">https://doi.org/10.1088/1755-1315/472/1/012027</a>

Kalambate, PK, Dar, RA, Karna, SP & Srivastava, AK 2015, 'High performance supercapacitor based on graphene-silver nanoparticles-polypyrrole nanocomposite coated on glassy carbon electrode', *Journal of Power Sources*, vol. 276, pp. 262-270, <a href="https://doi.org/10.1016/j.jpowsour.2014.11.130">https://doi.org/10.1016/j.jpowsour.2014.11.130</a>

Kumar, V, Gupta, RK, Gundampati, RK, Singh, DK, Mohan, S, Hasan, SH & Malviya, M 2018, 'Enhanced electron transfer mediated detection of hydrogen peroxide using a silver nanoparticle-reduced graphene oxide-polyaniline fabricated electrochemical sensor', *RSC Advances*, vol. 8, no. 2, pp. 619-631, <a href="https://doi.org/10.1039/c7ra11466d">https://doi.org/10.1039/c7ra11466d</a>

Kusrini, E, Suhrowati, A, Usman, A, Degirmenci, DV & Khalil, M 2019, 'Synthesis and characterization of graphite oxide, graphene oxide, and reduced graphene oxide from graphite waste using modified Hummers' method and zinc as reducing agent', *International Journal of Technology*, vol. 10, no. 6, pp. 1093–1104, <a href="https://doi.org/10.14716/jjtech.v10i6.3639">https://doi.org/10.14716/jjtech.v10i6.3639</a>

Lepak-Kuc, S, Wasilewska, K, Janczak, D, Nowicka, T & Jakubowska, M 2022, 'Conductive layers on a shrinkable PET film by flexographic printing', *Materials*, vol. 15, no. 10, article 3649, <a href="https://doi.org/10.3390/ma15103649">https://doi.org/10.3390/ma15103649</a>

Li, B-Q, Nie, F, Sheng, Q-L & Zheng, J-B 2015, 'An electrochemical sensor for sensitive determination of nitrites based on Ag-Fe3O4-graphene oxide magnetic nanocomposites', *Chemical Papers*, vol. 69, no. 7, pp. 911-920, <a href="https://doi.org/10.1515/chempap-2015-0099">https://doi.org/10.1515/chempap-2015-0099</a>

Li, R, Yang, T, Li, Z, Gu, Z, Wang, G & Liu, J 2017, 'Synthesis of palladium@gold nanoalloys/nitrogen and sulphur-functionalized multiple graphene aerogel for electrochemical detection of dopamine', *Analytica Chimica Acta*, vol. 954, pp. 43-51, <a href="https://doi.org/10.1016/j.aca.2016.12.031">https://doi.org/10.1016/j.aca.2016.12.031</a>

Li, Z-F, Zhang, H, Liu, Q, Liu, Y, Stanciu, L & Xie, J 2014, 'Covalently-grafted polyaniline on graphene oxide sheets for high performance electrochemical supercapacitors', *Carbon*, vol. 71, pp. 257-267, <a href="https://doi.org/10.1016/j.carbon.2014.01.037">https://doi.org/10.1016/j.carbon.2014.01.037</a>

Liu, L, Shen, Z, Zhang, X & Ma, H 2021, 'Highly conductive graphene/carbon black screen printing inks for flexible electronics', *Journal of Colloid and Interface Science*, vol. 582, pp. 12-21, <a href="https://doi.org/10.1016/j.jcis.2020.07.106">https://doi.org/10.1016/j.jcis.2020.07.106</a>

Liu, Y, Li, Q, Feng, Y-Y, Ji, G-S, Li, T-C, Tu, J & Gu, X-D 2014, 'Immobilisation of acid pectinase on graphene oxide nanosheets', *Chemical Papers*, vol. 68, no. 6, pp. 732-738, <a href="https://doi.org/10.2478/s11696-013-0510-x">https://doi.org/10.2478/s11696-013-0510-x</a>

Magdassi, S, Grouchko, M, Berezin, O & Kamyshny, A 2010, 'Triggering the sintering of silver nanoparticles at room temperature', *ACS Nano*, vol. 4, no. 4, pp. 1943-1948, <a href="https://doi.org/10.1021/nn901868t">https://doi.org/10.1021/nn901868t</a>

Mallakpour, S & Hussain, CM 2021, *Handbook of consumer nanoproducts*, Springer, Singapore, <a href="https://doi.org/10.1007/978-981-15-6453-6">https://doi.org/10.1007/978-981-15-6453-6</a>

Martinez-Lombardia, E, Gonzalez-Garcia, Y, Lapeire, L, De Graeve, I, Verbeken, K, Kestens, L, Mol, JMC & Terryn, H 2014, 'Scanning electrochemical microscopy to study the effect of crystallographic orientation on the electrochemical activity of pure copper', *Electrochimica Acta*, vol. 116, pp. 89-96, <a href="https://doi.org/10.1016/j.electacta.2013.11.048">https://doi.org/10.1016/j.electacta.2013.11.048</a>

Mekuye, B & Abera, B 2023, 'Nanomaterials: An overview of synthesis, classification, characterization, and applications', *Nano Select*, vol. 4, no. 8, pp. 486-501, <a href="https://doi.org/10.1002/nano.202300038">https://doi.org/10.1002/nano.202300038</a>

Mohanapriya, K, Ghosh, G & Jha, N 2016, 'Solar light reduced graphene as high energy density supercapacitor and capacitive deionization electrode', *Electrochimica Acta*, vol. 209, pp. 719-729, https://doi.org/10.1016/j.electacta.2016.03.111

Mooss, VA, Bhopale, AA, Deshpande, PP & Athawale, AA 2017, 'Graphene oxide-modified polyaniline pigment for epoxy based anti-corrosion coatings', *Chemical Papers*, vol. 71, no. 8, pp. 1515-1528, <a href="https://doi.org/10.1007/s11696-017-0146-3">https://doi.org/10.1007/s11696-017-0146-3</a>

Mousavi-Kamazani, M, Zarghami, Z & Salavati-Niasari, M 2016, 'Facile and novel chemical synthesis, characterization, and formation mechanism of copper sulfide (Cu2S, Cu2S/CuS, CuS) nanostructures for increasing the efficiency of solar cells', *Journal of Physical Chemistry C*, vol. 120, no. 4, pp. 2096-2108, <a href="https://doi.org/10.1021/acs.jpcc.5b11566">https://doi.org/10.1021/acs.jpcc.5b11566</a>

Murdiya, F, Hendri, YB, Hamzah, A, Frimayanti, N & Amri, A 2022, 'Few-layer wrinkled graphene (FLwG) obtained from coconut-shell-based charcoal using a high-voltage plasma method', *International Journal of Technology*, vol. 13, no. 1, pp. 157-167, <a href="https://doi.org/10.14716/ijtech.v13i1.4572">https://doi.org/10.14716/ijtech.v13i1.4572</a>

Nugrahaningtyas, KD, Kusrini, E, Salsabila, S, Fitriana, D, Usman, A, Kusumaningsih, T & Santoso, SJ 2025, 'Synthesis of transition metal-nanochitosan composites using Ni, Cu, Zn, and Ag metal ions and applications as antibacterial agents', *International Journal of Technology*, vol. 16, no. 1, pp. 207-220, <a href="https://doi.org/10.14716/ijtech.v16i1.6969">https://doi.org/10.14716/ijtech.v16i1.6969</a>

Nur, HM, Song, JH, Evans, JRG & Edirisinghe, MJ 2002, 'Ink-jet printing of gold conductive tracks', *Journal of Materials Science: Materials in Electronics*, vol. 13, no. 4, pp. 213–219, <a href="https://doi.org/10.1023/A:1014827900606">https://doi.org/10.1023/A:1014827900606</a>

Pandey, A & Qureshi, A 2017, 'Surface modified graphene oxide nanosheets by gold ion implantation as a substrate for surface enhanced Raman scattering', *Journal of Alloys and Compounds*, vol. 703, pp. 500-507, <a href="https://doi.org/10.1016/j.jallcom.2017.02.020">https://doi.org/10.1016/j.jallcom.2017.02.020</a>

Park, BK, Kim, D, Jeong, S, Moon, J & Kim, JS 2007, 'Direct writing of copper conductive patterns by inkjet printing', *Thin Solid Films*, vol. 515, no. 19, pp. 7706-7711, https://doi.org/10.1016/j.tsf.2006.11.142

Pegu, B, Konwar, M, Sarma, D & Konwer, S 2024, 'Cu nanoparticle anchored highly conducting, reusable multifunctional rGO/PANI nanocomposite: A novel material for methanol sensor and a catalyst for click reaction', *Synthetic Metals*, vol. 301, article 117516, <a href="https://doi.org/10.1016/j.synthmet.2023.117516">https://doi.org/10.1016/j.synthmet.2023.117516</a>

Petrovski, A, Paunović, P, Avolio, R, Errico, ME, Cocca, M, Gentile, G, Grozdanov, A, Avella, M, Barton, J & Dimitrov, A 2017, 'Synthesis and characterization of nanocomposites based on PANI and carbon nanostructures prepared by electropolymerization', *Materials Chemistry and Physics*, vol. 185, pp. 83-90, <a href="https://doi.org/10.1016/j.matchemphys.2016.10.008">https://doi.org/10.1016/j.matchemphys.2016.10.008</a>

Qiu, Z, He, D, Wang, Y, Zhao, X, Zhao, W & Wu, H 2017, 'High performance asymmetric supercapacitors with ultrahigh energy density based on hierarchical carbon nanotubes@NiO core-shell nanosheets and defect-introduced graphene sheets with hole structure', *RSC Advances*, vol. 7, no. 13, pp. 7843-7856, <a href="https://doi.org/10.1039/c6ra27369f">https://doi.org/10.1039/c6ra27369f</a>

Reddy, BN, Pathania, A, Rana, S, Srivastava, AK & Deepa, M 2014, 'Plasmonic and conductive Cu fibers in poly(3,4-ethylenedioxythiophene)/Cu hybrid films: Enhanced electroactivity and electrochromism', *Solar Energy Materials and Solar Cells*, vol. 121, pp. 69-79, <a href="https://doi.org/10.1016/j.solmat.2013.10.027">https://doi.org/10.1016/j.solmat.2013.10.027</a>

Saini, A, Madhuri, A, Sahoo, SK, Devi, PS, Jena, S, Laha, S & Swain, BP 2024, 'Investigation of microstructural, chemical bonding and optical properties of Fe-Cu/rGO nanocomposites', *Journal of Alloys and Metallurgical Systems*, vol. 5, article 100053, <a href="https://doi.org/10.1016/j.jalmes.2023.100053">https://doi.org/10.1016/j.jalmes.2023.100053</a>

Salamani, A, Merrouche, A, Telli, L, Gómez-Romero, P & Huertas, ZC 2018, 'Synthesis and caracterization of mesoporous FePO<sub>4</sub> as positive electrode materials for lithium batteries', *Surface Engineering and Applied Electrochemistry*, vol. 54, no. 1, pp. 55-63, <a href="https://doi.org/10.3103/S106837551801012X">https://doi.org/10.3103/S106837551801012X</a>

Sasri, R, Nurlina, Destiarti, L & Syahbanu, I 2018, 'Size analysis of silica particles extracted from solid rocks from Ketapang Regency, West Kalimantan', *Indonesian Journal of Pure and Applied Chemistry*, vol. 1, no. 1, pp. 39-43, <a href="https://doi.org/10.26418/indonesian.v1i1.26042">https://doi.org/10.26418/indonesian.v1i1.26042</a>

Shahriary, L, Nair, R, Sabharwal, S & Athawale, AA 2015, 'One-step synthesis of Ag-reduced graphene oxide-multiwalled carbon nanotubes for enhanced antibacterial activities', *New Journal of Chemistry*, vol. 39, no. 6, pp. 4583-4590, <a href="https://doi.org/10.1039/c4nj02275k">https://doi.org/10.1039/c4nj02275k</a>

Sharma, V, Jain, Y, Kumari, M, Gupta, R, Sharma, SK & Sachdev, K 2017, 'Synthesis and characterization of graphene oxide (GO) and reduced graphene oxide (rGO) for gas sensing application', *Macromolecular Symposia*, vol. 376, no. 1, article 1700006, <a href="https://doi.org/10.1002/masy.201700006">https://doi.org/10.1002/masy.201700006</a>

Shen, X, Zhao, S & Wan, A 2021, 'A sensitive and flexible sensor enhanced by constructing graphene-based polyaniline conductive networks', *Sensors and Actuators A: Physical*, vol. 330, article 112862, https://doi.org/10.1016/j.sna.2021.112862

Shishir, MKH, Afrin, S, Sachchu, MMH, Eva, TN, Tabassum, S, Ahmed, S, Sadia, SI & Alam, MA 2024, 'Crystalline copper nanomaterials for advanced ceramic: A comprehensive review for functional ceramic coating approaches', *Asian Journal of Advanced Research and Reports*, vol. 18, no. 8, pp. 13-34, <a href="https://doi.org/10.9734/ajarr/2024/v18i8706">https://doi.org/10.9734/ajarr/2024/v18i8706</a>

Singh, WI, Sinha, S, Devi, NA, Nongthombam, S, Laha, S & Swain, BP 2022, 'Fabrication and characterization of reduced graphene oxide/polyaniline/poly(caprolactone) electrospun nanofiber', *Arabian Journal for Science and Engineering*, vol. 47, no. 1, pp. 925-934, <a href="https://doi.org/10.1007/s13369-021-05901-3">https://doi.org/10.1007/s13369-021-05901-3</a>

Sonawane, A, Mujawar, MA & Bhansali, S 2019, 'Atmospheric plasma treatment enhances the biosensing properties of graphene oxide-silver nanoparticle composite', *Journal of the Electrochemical Society*, vol. 166, no. 9, pp. B3084-B3090, <a href="https://doi.org/10.1149/2.0161909jes">https://doi.org/10.1149/2.0161909jes</a>

Tien, H-W, Huang, Y-L, Yang, S-Y, Wang, J-Y & Ma, C-CM 2011, 'The production of graphene nanosheets decorated with silver nanoparticles for use in transparent, conductive films', *Carbon*, vol. 49, no. 5, pp. 1550-1560, <a href="https://doi.org/10.1016/j.carbon.2010.12.022">https://doi.org/10.1016/j.carbon.2010.12.022</a>

Trisnadewi, T, Kusrini, E, Nurjaya, DM, Paul, B, Thierry, M & Putra, N 2023, 'Comparison of phase change materials of modified soy wax using graphene and MAXene for thermal energy storage materials in buildings', *International Journal of Technology*, vol. 14, no. 3, pp. 596-605, <a href="https://doi.org/10.14716/ijtech.v14i3.6092">https://doi.org/10.14716/ijtech.v14i3.6092</a>

Valan, SL, De Cruz, AE, Jacob, PJ & Djearamane, S 2022, 'Sustainable synthesis of copper oxide nanoparticles using Aquilaria malaccensis (agarwood) leaf extract as reducing agent', *International Journal of Technology*, vol. 13, no. 5, pp. 1115-1125, <a href="https://doi.org/10.14716/ijtech.v13i5.5845">https://doi.org/10.14716/ijtech.v13i5.5845</a>

Vaseem, M, McKerricher, G & Shamim, A 2016, 'Robust design of a particle-free silver-organo-complex ink with high conductivity and inkjet stability for flexible electronics', *ACS Applied Materials and Interfaces*, vol. 8, no. 1, pp. 177-186, <a href="https://doi.org/10.1021/acsami.5b08125">https://doi.org/10.1021/acsami.5b08125</a>

Wang, Q, Yan, J & Fan, Z 2016, 'Carbon materials for high volumetric performance supercapacitors: Design, progress, challenges and opportunities', *Energy and Environmental Science*, vol. 9, no. 3, pp. 729-762, <a href="https://doi.org/10.1039/c5ee03109e">https://doi.org/10.1039/c5ee03109e</a>

Warsiki, E 2018, 'Application of chitosan as biomaterial for active packaging of ethylene absorber', *In:* IOP Conference Series: Earth and Environmental Science, vol. 141, no. 1, article 012036, <a href="https://doi.org/10.1088/1755-1315/141/1/012036">https://doi.org/10.1088/1755-1315/141/1/012036</a>

Wisudawaty, P, Djatna, T & Sugiarto 2024, 'Analysis and design of smart food packaging monitoring model based on chipless RFID sensor', *IOP Conference Series: Earth and Environmental Science*, vol. 1358, article 012038, <a href="https://doi.org/10.1088/1755-1315/1358/1/012038">https://doi.org/10.1088/1755-1315/1358/1/012038</a>

Wu, L, Hao, L, Pang, B, Wang, G, Zhang, Y & Li, X 2017, 'MnO2 nanoflowers and polyaniline nanoribbons grown on hybrid graphene/Ni 3D scaffolds by in situ electrochemical techniques for high-performance asymmetric supercapacitors', *Journal of Materials Chemistry A*, vol. 5, no. 9, pp. 4629–4637, https://doi.org/10.1039/c6ta10757e

Xu, Q, Gu, SX, Jin, L, Zhou, YE, Yang, Z, Wang, W & Hu, X 2014, 'Graphene/polyaniline/gold nanoparticles nanocomposite for the direct electron transfer of glucose oxidase and glucose biosensing', *Sensors and Actuators B: Chemical*, vol. 190, pp. 562-569, <a href="https://doi.org/10.1016/j.snb.2013.09.049">https://doi.org/10.1016/j.snb.2013.09.049</a>

Yao, Y 2022, 'Facile synthesis of copper-coated-reduced-graphene-oxide and its application as a highly sensitive electrochemical sensor for hydroquinone', *Journal of Chemistry*, vol. 2022, pp. 1-11, <a href="https://doi.org/10.1155/2022/6894049">https://doi.org/10.1155/2022/6894049</a>

Yi, Y, Samara, A & Wang, B 2021, 'A new approach for an ultra-thin piezoresistive sensor based on solidified carbon ink film', *Journal of Materials Science*, vol. 56, no. 1, pp. 607-614, https://doi.org/10.1007/s10853-020-05309-8